Hydrogen borrowing : towards aliphatic tertiary amines from lignin model compounds using a supported copper catalyst

Hydrogen borrowing: Towards aliphatic tertiary amines from lignin model compounds using a supported copper catalyst

Dieter Ruijten,[a] Thomas Narmon, [a] Hanne De Weer, [a] Robbe van der Zweep, [a] Claude Poleunis, [b] Damien P. Debecker, [b] Bert U.W. Maes, [c] Bert F. Sels*[a]

[a] D. Ruijten, H. De Weer, R. van der Zweep, Prof. Dr. B. F. Sels
Center for Sustainable Catalysis and Engineering
KU Leuven, Celestijnenlaan 200F, Leuven 3001 (Belgium)
E-mail: bert.sels@kuleuven.be

[b] Prof. Dr. D. P. Debecker
Institute of Condensed Matter and Nanosciences
Université Catholique de Louvain (UCLouvain)
1348 Louvain-La-Neuve, (Belgium)

[c] Prof. Dr. B. U. W. Maes
Organic Synthesis Division, Department of Chemistry
University of Antwerp, Groenenborgerlaan 171, Antwerp 2020 (Belgium)

Supporting information for this article is given via a link at the end of the document.

Abstract: Upcoming biorefineries, such as lignin-first provide renewable aromatics containing unique aliphatic alcohols. In this context, a Cu-ZrO_2 catalyzed hydrogen borrowing approach was established to yield tertiary amine from the lignin model monomer 3-(3,4-dimethoxyphenyl)-1-propanol and the actual lignin-derived monomers, (3-(4-hydroxyphenyl)-1-propanol and dihydroconiferyl alcohol), with dimethylamine. Various industrial metal catalysts were evaluated, resulting in nearly quantitative mass balances for most catalysts. Identified intermediates, side and reaction products were placed into a corresponding reaction network, supported by kinetic evolution experiments. Cu-ZrO_2 was selected as most suitable catalyst combining high alcohol conversion with respectable aliphatic tertiary amine selectivity. Low pressure H_2 was key for high catalyst activity and tertiary amine selectivity, mainly by hindering undesired reactant dimethylamine disproportionation and alcohol amidation. Besides dimethylamine model, diverse secondary amine reactants were tested with moderate to high tertiary amine yields. As most active catalytic site, highly dispersed Cu species in strong contact with ZrO_2 is suggested. ToF-SIMS, N_2O chemisorption, TGA and XPS of spent Cu-ZrO_2 revealed that imperfect amine product desorption and declining surface Cu lowered the catalytic activity upon catalyst reuse, while thermal reduction readily restored the initial activity and selectivity demonstrating catalyst reuse.

Introduction

Tertiary amines are an indispensable class of molecules, as they are widely used as building blocks of surfactants[1] and more generally, in polymer industry.[2] Furthermore, these functionalities are omnipresent as active ingredients in fine chemicals, such as agrochemicals and medicines, including many listed as essential by WHO.[3–5] It is estimated that 26% of all drugs and agrochemicals comprises a tertiary alkyl amine functionality.[6] Given their importance, numerous classical synthesis methods exist, starting from alkyl halides[7], nitriles[8], alkenes[9], amides[10], nitro[11] and carbonyl compounds.[12–14] Reductive amination, starting from aldehydes/ketones, which are *in situ* transformed into imines and subsequently reduced, is commonly used. However, carbonyl compounds are typically prepared from alcohols, thus demanding a separate upfront oxidation and an additional reductant during the reductive amination reaction. Both oxidant and reductant are required in at least stoichiometric amount. Direct alcohol amination by so-called hydrogen borrowing (HB) is a more appealing alternative.[15–17] Alcohols, which are mostly inexpensive[2] and easily accessible from renewable feedstock can be used directly here.[18,19] During HB, the alcohol is catalytically dehydrogenated to a more electrophilic carbonyl, followed by *in situ* condensation with an amine and consecutive reduction. During reduction, the imino or enamine is hydrogenated to the final amine, thereby consuming the hydrogen liberated in the oxidation step, hence the name hydrogen borrowing.[16,20] The excellent atom-efficiency, with ideally water as sole byproduct, makes this methodology highly appealing.[21] This dehydrogenation-condensation-hydrogenation process is commonly catalyzed by transition metal-based catalysts, both homogeneous (Ir[22,23], Ru[24–27], Cr[28], Fe[29], Mn[30], Ni[15]) and heterogeneous (Cu[31,32], Co[33,34], Ni[20,35,36], Pd[37], Ru[38,39]) as recently reviewed by Kempe *et al*.[40,41] N-alkylation of various alcohols has been reported, starting mostly from NH_3[20,33,35,38], and (C-substituted) anilines.[15,28–30,32] Disclosures dedicated to employing primary and secondary alkylamines exist, but are more scarce.[24,25,31]

With the blossoming biorefinery concept, including lignin-first lignocellulose depolymerization methodologies, bio-derived aryl substituted aliphatic alcohols are becoming abundantly available for downstream processing.[42–47] These lignin-derived aromatics, depending on the applied biorefinery strategy, can contain a 3-hydroxypropyl

side chain[48], thereby forming an attractive target for HB towards valuable tertiary amines, in particular *N,N*-dimethylamine derivatives. Surprisingly, whereas plenty of work has focused on amination of phenol moieties[49,50], research focusing on side-chain amination of such monomers is still lacking. Only recently, Barta *et al.* successfully reacted dihydroconiferyl and dihydrosinapyl alcohol with anilines using expensive homogeneous Shvo catalyst and with ammonia using Raney Nickel.[26] Previously, the same group presented a two-step amination pathway for dihydroconiferyl alcohol using ammonia and Ni-SiO_2/Al_2O_3 catalyst via a nitrile intermediate.[51] During their work on direct alcohol aminations, Baiker *et al.* demonstrated the gas-phase amination of 3-phenyl-1-propanol with dimethylamine (DMAn) by supported Cu catalysts.[31] Although 3-phenyl-1-propanol is structurally similar to lignin-derived monomers, it lacks the characteristic oxygenated moieties (i.e., methoxy and hydroxy). These groups bring chemical challenges as they can strongly coordinate to the catalyst surface, thereby hindering reaction.[26,52]

Side chain amination of these lignin-derived monomers could lead to valuable compounds, in particular antioxidant agents. Structurally similar phenol and amine derivatives are known for their antioxidant activity and are found in foods, lubricants, and polymers.[53] A physical mixture featuring a phenolic and tertiary amine functionality together can work synergistically, as they possess different selectivity towards various oxidation-derived radicals, thereby attacking different reactive pathways.[54] Moreover, combining the phenolic and amine moiety in a single molecule has been proven effective as well.[55,56] Conventionally, these (sterically hindered) phenolic alkylamines are synthesized in multiple steps, generally generating stoichiometric amounts of waste (Figure 1a and Figure S1). By starting from lignin-derived monomers, a more sustainable and bio-based antioxidant agent can be created, exploiting the inherent complexity of its parent lignin and hereby bypassing typical multistep approaches encountered with petrochemical-synthesis.

In this contribution, we studied liquid-phase heterogeneously catalyzed upgrading of the lignin model compound 3-(3,4-dimethoxyphenyl)-1-propanol (**1a,** Figure 1b) and the actual lignin-derived monomers, (3-(4-hydroxyphenyl)-1-propanol (**1p**) and dihydroconiferyl alcohol (**1g**), towards their *N,N*-dimethylamino derivatives via HB. Alcohol **1a** was initially used as readily available model compound (in comparison to dihydroconiferyl alcohol), mimicking the main structural aspects, *viz*. MeO-arene and aliphatic C3 primary alcohol, of lignin-first monomers. This ensures that potential negative effects linked to the oxygenated moieties (e.g., side reactions, metal coordinating ability) are taken into account as good as possible.[26,52] As this model compound lacks a phenolic group, the catalytic investigation strictly focuses on the amination of the primary alcohol side-group, as this is the goal of this contribution. In a second stage, the lignin-derived monomers were applied to demonstrate the general applicability of the developed HB protocol.

As a first step, a critical and large selection of heterogeneous transition metal-based catalysts was evaluated, putting forward an active and selective, commercially available Cu-ZrO_2 catalyst as highly suitable for HB. Under optimal conditions, the desired *N,N*-dimethyl-3-(3,4-dimethoxyphenyl)-1-propanamine (**2a**) was obtained with 97% selectivity at high conversion (95%). Important side products and intermediates were identified, and their evolution during the reaction monitored, resulting in nearly quantitative mass balances and a comprehensive reaction scheme. Furthermore, the scope of the developed methodology on **1a** was determined with various aliphatic and aromatic secondary amine reactants. Importantly, the developed methodology could easily be extended to lignin monomers **1p** and **1g** with excellent alcohol conversion (98% and 86%, resp.) and high selectivity towards the tertiary amine (87% and 91%, resp.).

Next, the structure activity relationship between copper and the zirconia support was examined, indicating the highest catalytic activity is displayed by finely dispersed Cu particles in strong contact with the zirconia support. In a final stage, catalyst reusability and deactivation was examined by recycling experiments, ToF-SIMS, N_2O chemisorption, TGA and XPS analysis, shedding light upon the main deactivation mechanism and demonstrating an effective catalyst regeneration strategy.

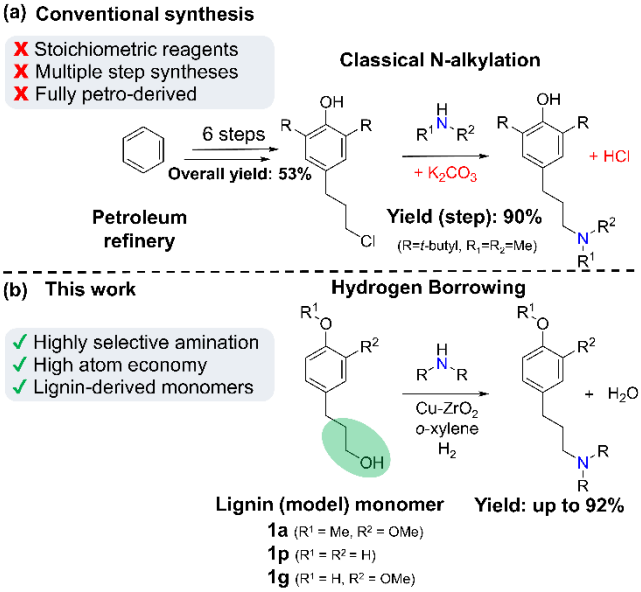

Figure 1. Conventional, multistep syntheses for the construction of (hindered) phenolic alkylamines and their disadvantages. b) The overall concept for synthetizing tertiary amines from lignin model compound **1a** with secondary amines, following a HB strategy.

Results and Discussion

Catalyst exploration

Whereas little research is done on the amination of lignin model compounds, amination of lower alcohols is a common industrial process.[2] Therefore, we started by evaluating multiple industrial heterogeneous non-precious (Cu, Ni, Co) and precious (Pd, Ru) metal-based catalysts for the HB of 3-(3,4-dimethoxyphenyl)-1-propanol (**1a**) with DMAn, providing *N*,*N*-dimethyl-3-(3,4-dimethoxyphenyl)-1-propanamine (**2a**), as shown in Table 1 and Figure S2. The mechanism of formation of **2a** and the side products observed is discussed in a separate section (*vide infra*).

Prior to reaction, each catalyst is pretreated as described in the experimental section and a fixed amount of catalyst (120 mg, 0.6 wt% *versus* total loading) was added to the reaction mixture, regardless of metal loading. *O*-xylene is applied as solvent since apolar, non-hydrogen bonding solvents (e.g., toluene, xylenes or aliphatic hydrocarbons) are commonly used during HB involving substrates containing aromatic entities.[20,22,27,57] They are able (i) to dissolve the substrates and products reasonably well and (ii) do not interfere strongly with the catalysts' active sites due to their low or absence of Lewis basicity.[58] For most catalysts, we were able to identify nearly all reaction products, thereby capable of reporting almost the complete mass balances. When no catalyst was used, no conversion of **1a** was detected pointing to thermal stability of substrate in *o*-xylene. Catalysts based on Co or expensive noble metals, such as Pd or Ru, performed poorly. As shown in Table 1, Co-Al_2O_3 (entry 1) and Pd-C (entry 2) were even inactive under the applied conditions. Co-Al_2O_3 has previously been applied as effective catalyst for the amination of aliphatic alcohols with ammonia.[59] However, alcohol conversion is reported to drop sharply at increased amine equivalents and low H_2 pressure, likely due to catalyst deactivation.[59,60] For Pd-C, it was proven that an additional (stronger) base is necessary for alcohol amination to occur, rationalizing why no conversion was obtained.[61] Pd-Al_2O_3 (entry 3), Ru-Al_2O_3 (entry 4) and Ru-C (entry 5) gave only minor amounts of the desired tertiary amine **2a**. For Ru-C, Ruiz *et al.* reported comparable conversion (38%) after 20 h (200 mg Ru/C, 150 °C, 0 bar H_2) for the HB of dodecanol with NH_3 (4 bar).[62] It is noteworthy that Pd-Al_2O_3 substantially displayed both undesired decarbonylation and hydrogenolysis activity, leading to 4-ethyl-1,2-dimethoxybenzene (**8a**) and 1,2-dimethoxy-4-propylbenzene (**9a**), respectively. Ru-Al_2O_3 yielded

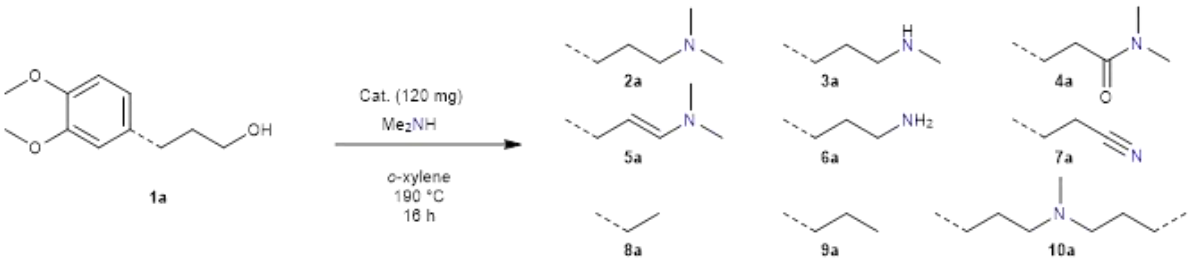

Entry	Catalyst	M / wt%	Conv. / %	Selectivity / %									MB / %
				2a	**3a**	**4a**	**5a**	**6a**	**7a**	**8a**	**9a**	**10a**	
1	Co-Al_2O_3	15	0	0	0	0	0	0	0	0	0	0	100
2	Pd-C	5	0	0	0	0	0	0	0	0	0	0	100
3	Pd-Al_2O_3	5	15	29	5	0	0	0	0	11	27	0	96
4	Ru-Al_2O_3	5	4	27	0	0	32	0	0	0	0	0	98
5	Ru-C	5	22	62	6	2	0	0	0	4	0	0	94
6	Raney Ni	95	83	55	24	0	0	10	2	0	0	5	99
7	Ni-SiO_2	50	92	56	20	1	0	10	4	1	0	2	97
8	Ni-SiO_2	55	78	56	20	1	0	12	6	<1	0	6	100
9	Ni-SiO_2	60	97	48	12	2	<1	2	7	1	0	8	90
10	Ni-Al_2O_3	17	81	48	8	4	1	2	2	5	0	4	94
11	Ni-Al_2O_3	21	96	54	13	7	0	1	7	1	0	6	95
12	Ni-Al_2O_3	32	97	45	13	7	0	4	9	1	0	6	91
13	Cu-SiO_2/CaO	26[b]	31	86	12	3	0	0	0	0	0	2	100
14	Cu-SiO_2/Al_2O_3	47[b]	65	70	12	4	0	1	0	0	0	1	92
15	Cu-SiO_2	59[b]	57	62	2	0	0	3	0	0	0	0	84
16	Cu sponge	98[b]	38	72	29	0	0	0	0	0	0	0	100
17	Cu sponge Zr	96[b]	60	80	20	<1	0	1	0	0	0	1	100
18	Cu-ZrO_2	43[b,c]	89	62	29	6	0	2	0	0	0	1	100

[a] Reaction conditions: 1 mmol **1a**, 20 mmol DMAn, *o*-xylene, 190 °C, 16h, 120 mg catalyst. Conversion and selectivities are determined by GC-FID. [b] Measured by WRD-XRF. [c] Active surface Cu metal content being 3.9 wt% of the catalyst as measured by N_2O chemisorption. M = Total metal content. MB = Mass balance.

the enamine **5a** as major product, implying a reduced C=N hydrogenation tendency. The tested Cu- and Ni-based catalysts were most active for HB. Generally, Ni-based catalysts (entry 6-12) from the Pricat® (Ni-SiO_2), HTC® (Ni-Al_2O_3) and Raney® (sponge Ni) series were more active compared to Cu-based catalysts (entry 13-18) as indicated by the higher conversion. However, Ni-based catalysts displayed greater selectivity towards **6a**, **7a** and **8a**, indicating their ability of secondary amine disproportionation, primary amine dehydrogenation[63], and decarbonylation (C-C bond cleavage). Within the Ni catalyst family, Ni-Al_2O_3 (21 wt%) (entry 11) showed the highest **2a** yield, corresponding to 52%.

For all tested Cu catalysts, selectivity towards desired **2a** was generally higher compared to Ni-based ones, with values clearly surpassing 60%. Remarkably, with Cu catalysts some minor amounts of amide **4a** were also detected. The best selectivity towards the tertiary amine **2a** was obtained by Cu-SiO_2/CaO, (86%, entry 13),

although at a modest alcohol conversion (31%). Zr-promoted Cu sponge (entry 17) showed similar selectivity towards **2a** (80%), but at double **1a** conversion (60%), thereby also outperforming non-Zr promoted sponge Cu (entry 16). The role of zirconium as promotor is to improve thermal stability and reduce metal sintering.[64] The most active Cu catalyst (89% conversion), also displaying decent selectivity towards **2a** (62%), was Cu-ZrO_2 (entry 18), thereby leading to the highest overall yield (55%) of **2a**. ZrO_2 as support has been reported for successful HB in combination with Au[65], Cu[66] and Ni[20]. The combination of weak to moderate acidic and basic surface sites[20,67] and the presence of oxygen vacancies[68] in ZrO_2 have been proposed as key properties beneficial for the HB reaction.

To correct for possible effects related to simply higher conversion rates among the catalysts, conversion *versus* **2a** selectivity plots for the three most promising Cu catalysts (Cu-SiO_2/CaO, Cu sponge Zr and Cu-ZrO_2) were constructed (Figure S3). The conversion *versus* selectivity plots further highlights the superior performance of the Cu-ZrO_2 catalyst, combining favourable selectivity and excellent conversion rates. For this reason, it was selected for further studying the HB of **1a**.

To gain further insight into the role of the catalyst, we performed some control experiments. General procedure 1 was followed using CuO-ZrO_2 pre-catalyst without prior reductive pretreatment. Conversion of **1a** did not take place, indicating the necessity of Cu^0 for the reaction to take place. Powder XRD pattern of the CuO-ZrO_2 pre-catalyst before reduction illustrated the absence of metallic Cu^0, while after reduction at 300 °C under H_2 flow, its signature reflection was clearly present (Figure S4). The heterogeneous nature of the reaction was verified by measuring Cu leaching by ICP analysis and a so-called "hot-filtration" test. For ICP analysis, a reaction according to General procedure 1 was performed and the crude mixture was filtered and concentrated *in vacuo*. The residue was digested and analyzed as described in the Experimental section. Low amount of Cu, *viz.* 5 ppm (for reaction under N_2) and 2 ppm (reaction under 1 bar H_2), corresponding to 0.2 wt% and 0.06 wt% of the Cu, respectively, was leached into reaction solvent. Moreover, results from the hot filtration for Cu-ZrO_2 show no product formation after the catalyst removal, indicating that leached Cu is not involved in the reaction and homogeneous catalysis can be excluded. Also, the absence of film diffusion limitations at the applied reaction conditions (stirring rate of 1400 rpm) was confirmed by conducting General procedure 1 at varying stirring speeds (Figure S5). For identical reaction times, substrate conversion remained constant above stirring rate of 1000 rpm.

Parameterization study for yield improvement

Encouraged by the above results, we continued investigating the major parameters that influence conversion rate and yield of HB of **1a** with DMAn employing the Cu-ZrO_2 catalyst.

A first important parameter is the catalyst loading. As long as free of diffusion limitations, increasing catalyst loading should improve the conversion rate until secondary reactions, following the first dehydrogenation step, become rate determining and dehydrogenation becomes an equilibrium reaction. To test if this equilibrium stage was already reached, the initial conversion rate (r_0) were determined from the initial linear part of the kinetic plot for various catalyst loading (20-180 wt% *versus* **1a**). As seen in Figure S6, a linear increase in r_0, related to the increased number of active sites, proves dehydrogenation has not yet reached equilibrium within the tested range and remains rate limiting. In the next experiments, a Cu-ZrO_2 loading of 120 mg (60 wt%) was applied.

A second parameter is the amine concentration, which might influence selectivity by quickly reacting with the otherwise reactive aldehyde intermediate, and by impacting amine disproportionation. Results are displayed in Figure 2a, where amine loadings are expressed in DMAn to **1a** equivalents. An optimal selectivity of 87% was obtained when 2 equivalents DMAn were applied. An amine to **1a** ratio of 1 gave similar selectivity towards the tertiary amine, but alcohol conversion was halved. At this low conversion, traces of the enamine **5a** were detected. Further raising the DMAn concentration above 2 equivalents did not affect the conversion, likely because dehydrogenation is rate determining. On the contrary, selectivity towards the tertiary amine declined with increasing DMAn excess in favor of the amide **4a**. During amide formation, it is likely that DMAn fulfils the role of a weak base, an essential additive during dehydrogenative alcohol amidation.[69] Moreover, hemiaminal **1''a** dehydration towards enamine **5a** is promoted by acid catalysis, hence increasing concentration of a DMAn (weak base) enhances the competing amide formation **4a** (Scheme 1).[70]

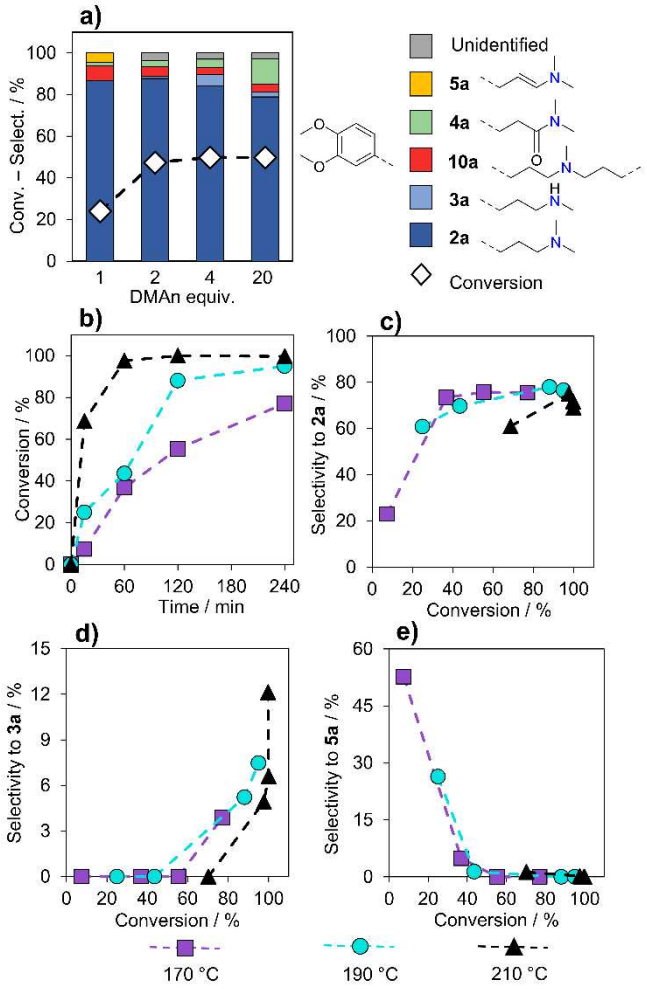

Figure 2. Influence of (a) DMAn equivalents and (b-e) temperature on **1a** conversion and selectivity towards the (c) tertiary amine (**2a**), (d) secondary amine (**3a**) and (e) enamine (**5a**). Reaction conditions: 1 mmol **1a**, DMAn, *o*-xylene, N_2, Cu-ZrO_2 (7 mol%, active Cu). Panel a): 190 °C, 1h. Panel (b-e) 2 mmol DMAn.

Temperature has an impact on both thermodynamics, and thus equilibria (Le Chatelier's Principle), and kinetics (Arrhenius). For the rate determining dehydrogenation, being endothermic, increasing temperature means more favorable conversion. Furthermore, all reaction rates will increase with temperature in accordance with their activation energy, as described by Arrhenius. This could affect **2a** yields ultimately. After all, equilibria of other side-reactions are obviously also influenced by temperature. With the optimal DMAn equivalents and loading of the catalyst set, the effect of reaction temperature and time was assessed (Figure 2b-e). Under the applied conditions, the reaction rate increased clearly with temperature (Figure 2b). By approximating initial conversion rates at the lowest conversion measured, we observed roughly a nine-fold increase in initial conversion rate by a 40 K temperature increase, corresponding to an apparent activation energy of 100 kJ/mol. The initially chosen reaction temperature of 190 °C led to nearly full conversion (95%) after 4 hours, while incomplete conversion was observed after 4 ours at 170°C. By raising the earlier chosen reaction temperature to 210 °C, full conversion was already obtained after 1 h. The impact of the temperature on selectivity is best compared at isoconversion. Highest selectivity (78%) is obtained at almost complete conversion, but care has to be taken not to keep the reaction at too long contact times as the selectivity could drop due to formation of the secondary amine **3a** (Figure 2d). For Cu catalysis, it is known that alkylamine disproportionation occurs at these temperatures (170-210 °C), yielding monomethylamine (MMA) and trimethylamine (TMA) starting from DMAn (Scheme 1b).[71] Coupling of the aldehyde intermediate with MMA will lead to secondary amine **3a**. Interestingly, this amine is formed especially at elevated alcohol conversion while being absent at low conversion, illustrating the suppressing effect of the alcohol on DMAn disproportionation.[72] A control experiment following General procedure 1, starting from pure tertiary amine **2a** without alcohol in presence of 2 equivalents DMAn and Cu-ZrO_2 catalyst (190 °C, 4 h) did not yield any secondary amine **3a**. This proves that the tertiary amine **2a** itself is not susceptible to disproportionation. Enamine **5a** (Figure 2e) and aldehyde **1′a** (Figure S7b) are only predominant at initial alcohol conversion, indicating their intermediate nature, and thus their kinetic profile is similar for the different temperatures. The amide **4a** profile ranged from 6-14% for the various conditions, with no distinctive trend for the tested temperatures

(Figure S7a). Overall, **1a** can be converted towards high conversion with a maximum selectivity at 78%, **3a** and **4a** being the most important side-products. 190 °C was selected as suitable temperature for following experiments, allowing to obtain nearly full conversion within a reasonable reaction time, combined with the best **2a** selectivity.

A fourth key parameter that may have several important consequences on HB is the hydrogen pressure. Although its presence can affect unfavorably the thermodynamics of dehydrogenation, it also can impact the selectivity towards **2a** by rapid hydrogenation of the enamine **5a**. In addition, the presence of hydrogen creates a reducing environment, potentially stabilizing the active metallic Cu^0 sites for dehydrogenation. Therefore, the optimal hydrogen pressure is substrate- and catalyst-dependent and needs fine-tuning. To examine the influence of hydrogen, the H_2 pressure was varied (in the range of 0 to 8 bar), while the total initial pressure, compensated with nitrogen, was kept constant at 10 bar. The reaction was monitored by taking aliquots over time. Although additional H_2 is in essence nonessential, from Figure 3a it can be observed that adding H_2 substantially improves selectivity towards the tertiary amine **2a**. At low alcohol conversion selectivity greatly improves towards the desired amine for all hydrogen pressures examined (1-8 bar), mainly by reducing **5a** formation (Figure 3b). The maximum enamine selectivity decreases with raising hydrogen pressure as it facilitates hydrogenation towards amine **2a**. Figure 3c shows that in contrast to a full nitrogen atmosphere, small amounts of secondary amine are already formed at lower conversion when hydrogen is added. However, the lowest H_2 pressure (1 bar) significantly reduces the secondary amine (**3a**) selectivity at elevated conversion (>80%) by suppressing DMAn disproportionation. Additional H_2 also effectively minimizes amide **4a** formation, even at the lowest pressure (Figure 3d). The latter results provides additional support that a second dehydrogenation step occurs during disproportionation[71,73] towards **3a**, and during amidation[69,70] towards **4a**, which is consistent with previous studies.

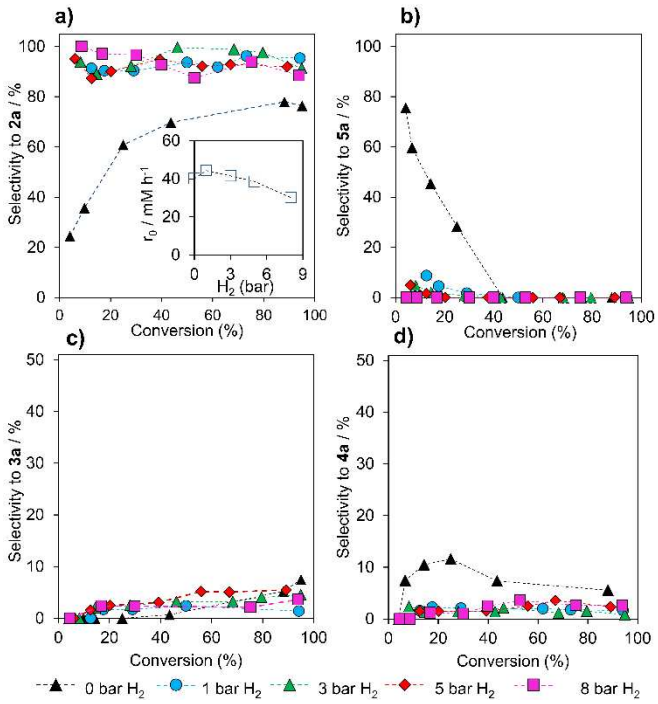

Figure 3. Influence of hydrogen pressure on conversion of **1a** and selectivity towards (a) tertiary amine **2a**, (b) enamine **5a**, (c) secondary amine **3a**, and (d) amide **4a**. Insert (a) shows the effect of H_2 on the initial conversion rate of **1a**. Reaction conditions: 1 mmol **1a**, 2 mmol DMAn, *o*-xylene, 10 bar total pressure (H_2 + N_2), Cu-ZrO_2 (7 mol%, active Cu) at 190 °C

Values of r_0 of **1a** were determined for different H_2 pressures using the initial linear part of the kinetic plots (Figure S8), and plotted against the hydrogen pressure in the insert of Figure 3a. Applying 1 bar H_2 increases r_0 when compared to reaction in a pure N_2 atmosphere. This rate at 1 bar hydrogen pressure represents the highest rate, equalling 44 mM h^{-1}. As a dehydrogenation takes place during HB, an adverse effect of H_2 on the rate might be expected as was observed here for elevated pressures (>3 bar). Further increasing H_2 pressure to 8 bar indeed lowered r_0. However, low pressure of H_2 (1 bar) likely helps to keep Cu catalyst in its active, reduced oxidation state zero. Previous studies also pointed out the importance of H_2 in minimizing catalyst deactivation.[60,71] In summary, working under low pressure hydrogen improves selectivity towards the tertiary amine **2a** by minimizing amide **4a** formation, enhancing enamine **5a** hydrogenation, and significantly suppressing DMAn

disproportionation, hereby reducing secondary amine (**3a**) formation. The effect is found to be similar for all investigated hydrogen pressures (1-8 bar) compared to HB in a full nitrogen atmosphere. Besides selectivity, r_0 also profits from low pressure hydrogen with an optimum at 1 bar, likely because the external hydrogen helps to keep the Cu catalyst in its active metallic form.

Reaction scope

Having the optimized HB reaction conditions for **1a** with DMAn in hand, we determined the scope of the method by using various aliphatic and aromatic secondary amines (Table 2). Aliphatic unbranched secondary dialkylamines (entry 1-5, Table 2) displayed good to excellent conversion (61-95%), which decreased with increasing alkyl chain length. A pronounced increase in selectivity towards the secondary amine side-product **3** was seen when diethyl-, dipropyl- or dibutylamine were used as amine reactant. This can be rationalized by the higher disproportionation reactivity of the larger dialkylamines. During metal-catalyzed disproportionation of dialkylamines, an initial dehydrogenation step is occurring, resulting in an imine (Scheme 1b).[71,73] It is likely that this step occurs more readily if more stable substituted imines (i.e., with larger alkyl chains) are formed. Besides, DMAn is a much stronger nucleophile than MMA for the condensation with the aldehyde, roughly 580 times, whereas this difference reverses with increasing alkyl chain length due to a steric effect. Dipropylamine, for instance is four times less nucleophilic relative to monopropylamine,[74,75] and thus less reactive in forming the hemiaminal addition intermediate.

For cyclic aliphatic amines (entry 6-9), the tertiary amine was always obtained with excellent selectivity (86-95%) and high conversion (72-97%), with nearly full conversion for pyrrolidine (entry **6**). Remarkably, no secondary amines **3** or dimer products **10** are formed for these cyclic amines (entry 6-9), as secondary amine disproportionation in these cases would involve ring-opening.[76] *N*-alkyl secondary anilines (entry 10-11), perform poorly, both in terms of conversion (≤ 23%) and tertiary amine selectivity (≤ 15%). The tertiary amine yield is slightly improved by adding an electron-donating *para*-methoxy moiety to the aromatic ring (entry 10 *vs.* 12), making the nitrogen more nucleophilic. Conversion (67%) and selectivity (71%) to the desired amine were higher for the more nucleophilic benzylamine (entry 13)**.** Noteworthy, *N*-methylanilines and *N*-methylbenzylamine follow different trends during secondary amine disproportionation. *N*-alkylanilines (entry 10-12) yield secondary amines with a *N*-aryl group (**3j, 3k**) as major side product (12-32% selectivity). With *N*-methylbenzylamine (entry 13) the major side product is **3a** (18% selectivity) and only 2% **3m** containing a *N*-benzyl moiety. Likely, the more stable conjugated imine formed during disproportionation of the *N*-methylbenzylamine favors the loss of the benzyl rather than the alkyl group. Noteworthy, for *N*-alkyl secondary aromatic amines, aldol addition reaction products (**11a,** Table 2) of aldehyde **1'a** were detected together with trace amounts of the aldehyde itself. Both observations suggest aldehyde accumulation and thus a slow nucleophilic addition reaction of aromatic amine relative to the aldehyde formation. It is clear that the initial amine structure has a significant effect on **1a** conversion and the product selectivity. Nucleophilic aliphatic secondary amines with smaller groups are preferred over *N*-alkyl aromatic anilines.

Table 2. Tertiary amines via HB of **1a** with various secondary amines[a].

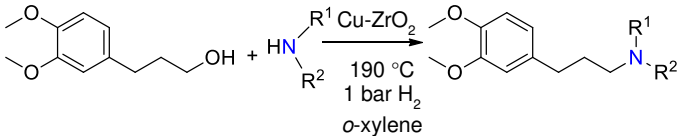

Entry	Amine		C / %	Selectivity / %				
				3° amine	2° amine	Amide		
				2	**3**	**4**	Dimer **1011a** [g]	
1		**a**	95	97	1	2	0	0
2		**b**	78	42	39	0	14	0
3		**c**	77	37	34	0	13	0
4		**d**	61	37	42	0	16	0
5		**e**	72	42[b]	18[c]	0	12	0
6		**f**	97	89	0	5	0	0
7		**g**	87	93	0	2	0	0
8	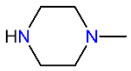	**h**	72	86	0	6	0	0
9		**i**	82	95	0	3	0	0
10	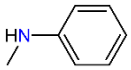	**j**	23	15	12[d]	0	0	20
11	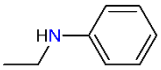	**k**	22	3	22[d]	0	0	27
12	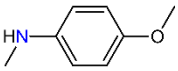	**l**	30	36	32[e]	0	0	16
13	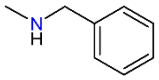	**m**	67	71	18 (2)[f]	1	0	10

[a] Reaction conditions: 1 mmol **1a**, 2 mmol amine, Cu-ZrO_2 (7 mol%, active Cu) 1 bar H_2, 190 °C for 5 h. [b] Selectivity to *N*-butyl-*N*-methyl-3-(3,4-dimethoxyphenyl)-1-propanamine (**2e**). Trace amount detected of **2a** and **2d**. [c] Selectivity towards *N*-butyl-3-(3,4-dimethoxyphenyl)propan-1-amine (**3d**). Trace amounts of **3a** were detected. [d] R-NH-aryl **3j**. [e] R-NH-aryl **3l.** [f] Selectivity towards **3a**. Selectivity towards R-NH-benzyl (**3m**) in parentheses. [g] Aldol addition product. R represents a 3-(3,4-dimethoxyphenyl)-1-propyl group. C = Conversion

Reaction network

Valuable insights towards the construction of a reaction network of parallel and consecutive reactions were gathered during the foregoing experiments by (i) varying the operational parameters,

(ii) extensive intermediate and side product identification and (iii) their kinetic profiling. This allowed identifying the most critical steps with regard to conversion rate and selectivity. All these reactions are summarized in Scheme 1a for the reaction of **1a** with DMAn. The desired pathway starts with the aliphatic alcohol **1a** dehydrogenation,

catalyzed by Cu-ZrO_2, giving rise to the corresponding aldehyde **1'a** intermediate as proven by its kinetic profile (Figure S7b). Metallic Cu is essential for this step as unreduced CuO-ZrO_2 was proven to be inactive. Additionally, a too high hydrogen pressure will negatively affect the equilibrium of this initial dehydrogenation step. For nucleophilic amines (*e.g.,* DMAn, pyrrolidine), fast nucleophilic addition of the amine on the reactive aldehyde yields hemiaminal **1''a**, resulting in a consistently low aldehyde concentration. For less nucleophilic amines (*e.g., N*-alkylanilines), aldehyde **1'a** accumulation takes place as a result of the slower carbonyl addition rate. As a result, undesired aldol addition reaction product **11a** can be formed, aided by the *N*-alkylanilines acting as a base rather than a nucleophile.[77] Once the hemiaminal **1''a** is formed, it converts to enamine **5a** via water elimination. Amide **4a** can also be formed competitively from the hemiaminal **1''a** by an additional dehydrogenation, explaining the lower **4a** selectivity at increasing H_2 pressure (Figure 3d). Metal-catalyzed synthesis of amides directly from alcohols and amines via dehydrogenation is a well-studied reaction.[78] Enamine **5a** hydrogenation yields the final desired tertiary amine **2a**. As observed, external hydrogen enhances this hydrogenation step, whereas a lack of it leads to temporarily enamine accumulation (Figure 3b).

Secondary amine **3a** and primary amine **6a** originate from disproportionation of reactant DMAn, which has been studied before.[71,72] DMAn disproportionation is a reaction initiated by dehydrogenation of DMAn followed by a DMAn attack, providing an aminal intermediate, which is subsequently hydrogenolyzed ultimately creating a mixture of MMA and TMA (Scheme 1b). Similarly, MMA itself can disproportionate, giving rise to NH_3 and DMAn. The reductive condensation of MMA and NH_3 with **1'a** yields **3a** and **6a**, respectively. MMA disproportionation is a minor reaction, and thus does not significantly affect the product outcome. As the initial step during reactant amine disproportionation involves a dehydrogenation, elevated hydrogen pressure effectively lowers the undesired amine disproportionation. (Figure 3c). As indicated by Figure 2d, disproportionation predominantly occurs at elevated alcohol conversion, hinting the catalyst's preference for alcohol over amine dehydrogenation, the first step in disproportionation. The secondary amine **3a** itself can condense with aldehyde **1'a** forming dimer **10a** upon imine hydrogenation. As demonstrated, reaction product **2a** itself does not disproportionate under the applied reaction conditions, as it lacks a free hydrogen on nitrogen. An additional control experiment was performed to verify the possible role of water, which is formed during HB of **1a,** on amine disproportionation (See Note 1 ESI). For this, General procedure 1 was followed, but 2 equivalents of water (*versus* **1a**) were added to the reaction mixture. Compared to the reference reaction (Table 1, amine **a**), no additional secondary amine product was formed. Remarkably, conversion dropped significantly (52% *versus* 95%), while selectivity to tertiary amine **2a** was identical (96%). The negative effect of water can be ascribed to (i) the shift in reaction equilibrium of imine formation through condensation according to Le Chatelier's Principle and (ii) the potential catalyst deactivation by formation of catalytic inactive copper hydroxides.

Looking at nitrile **7a**, which was exclusively formed in presence of Ni-based catalysts, dehydrogenation of primary amine **6a** is suggested as most plausible pathway.[63] Pd-Al_2O_3 is the only tested catalyst exhibiting hydrogenolysis activity, resulting in **9a** (Table 1). Besides for Cu-based catalysts, decarbonylation of **1'a** to **8a** cannot completely be prevented for the other tested transition metal catalysts (Table 1).[79]

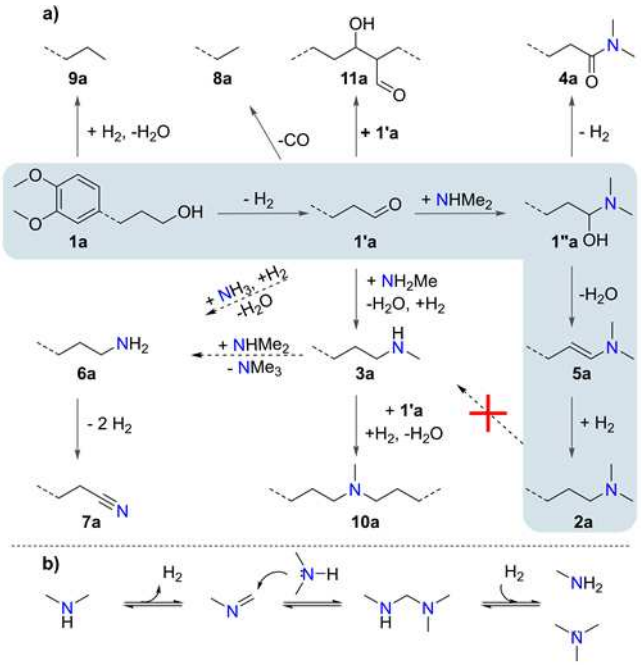

Scheme 1. Plausible reaction network for a) the metal catalyzed amination of **1a** with DMAn via HB and b) disproportionation reaction of DMAn taking place during amination of **1a** with DMAn in presence of a Cu or Ni based catalyst, based on ref [71,73]

Lignin monomer amination

Having this selective amination method in hand, we moved to the HB of the actual lignin-derived monomers, 3-(4-hydroxyphenyl)-1-propanol **1p** (entry 1, Table 3) and dihydroconiferyl alcohol **1g** (entry 2, Table 3) with DMAn. Good to excellent conversion of the monomers of 98% (**1p**) and 86% (**1g**), respectively, are obtained under the optimized conditions with a high selectivity to the desired *N*,*N*-dimethylamino compound. The tertiary amine yield (78%) for the amination of lignin monomer **1g** with DMAn using the supported Cu-ZrO_2 catalyst exceeds the previously reported yield (53%) obtained with a homogeneous Ru catalyst.[26] It is noteworthy that no amination of the phenolic moiety was detected for **1p** and **1g**. Amination of the phenol requires a partial hydrogenation of the aromatic ring, which is typically catalyzed by supported Pd or Ni catalyst instead of Cu.[80,81]

Table 3. HB of **lignin monomer** with DMAn using Cu-ZrO_2 catalyst [a].

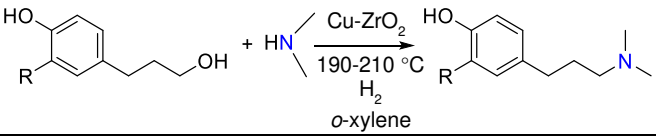

Entry	Substrate		Conv. [c] \ %	Sel. [c] \ %
1	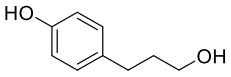	**1p**	98 (75)	87 (67)
2[b]	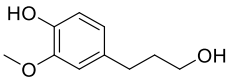	**1g**	86 (66)	91 (58)

[a] Reaction conditions: 1 mmol alcohol, 2 mmol DMAn, 120 mg Cu-ZrO_2 (43 wt% Cu), 1 bar H_2, 190 °C for 4 h. [b] 210 °C, 16h, 3 bar H_2. [c] values in parentheses are obtained by using in house made Cu-ZrO_2 (120 mg, 5 wt% Cu) catalyst.

Catalyst metal loading

Typically, industrial Ni- and Cu-based supported catalyst have a relative high metal loading (Table 1). By increasing the metal loading, the metal-support interface decreases while the metal particle size increases. Previously, the metal-support interface has been suggested as active site for the HB reaction.[20,82] To assess the role of the Cu metal loading on the catalytic performance, additional Cu-ZrO_2 catalysts with varying Cu loading (2.5, 5.0, 10.0, 15.0 wt%) were prepared by incipient wetness impregnation as described in the experimental section. The activities of the commercial and the self-prepared catalysts were evaluated as shown in Figure 4, where the TOF of the alcohol substrate conversion per surface active Cu atom was given in function of the ZrO_2 to Cu ratio. As shown, TOF per surface active Cu site increases linearly along the ZrO_2 to Cu ratio, reaching a plateau at around 20 (*i.e.*, 5 wt% Cu). ZrO_2 without Cu showed no catalytic activity. TPR profiles (Figure S11) of the various catalyst showed a single reduction peak centered around 215 °C for the catalyst with the highest TOF (2.5 wt% and 5 wt% Cu loading), indicating one- and two-dimensional highly dispersed surface copper species (See also Table S2). Upon further increasing the Cu loading (> 5wt%), a second peak arises centered around 250-270 °C, representing larger three-dimensional bulk copper clusters.[83,84] This implies that the dispersion capacity of ZrO_2 is around 5 wt% Cu and that higher Cu loadings result in the formation of bulk CuO.[84,85] Overall, these results indicate that highly dispersed Cu particles and the corresponding Cu-ZrO_2 interphase is key to high TOF during HB. Similarly, Shimizu *et al.* suggested the metal/support interface in Ni-Al_2O_3 as active site for HB of secondary alcohols [20,82].

As the Cu-ZrO_2 (5wt%) displayed the highest TOF per surface active Cu site and the highest initial activity by catalyst weight (measured at low conversion of **1a**,<40%), it was tested for the amination of lignin monomers **1p** and **1g** with DMAn under the previously optimized conditions (Table 3, in parentheses). Compared to the commercial Cu-ZrO_2 (43 wt%) catalyst, conversion of the monomer and selectivity towards the tertiary amine product were slightly lowered. Despite Cu-ZrO_2 (5 wt%) having the most active Cu sites, it is plausible that the lower total amount of surface active Cu species renders it more susceptible to catalyst deactivation by the strongly coordinating phenolic monomers, and a compromise between activity and stability needs to be decided here. Further improving the exploitation of these highly active Cu sites for the HB of lignin-derived compounds thus remains a challenge with regard to catalyst stability for future research.

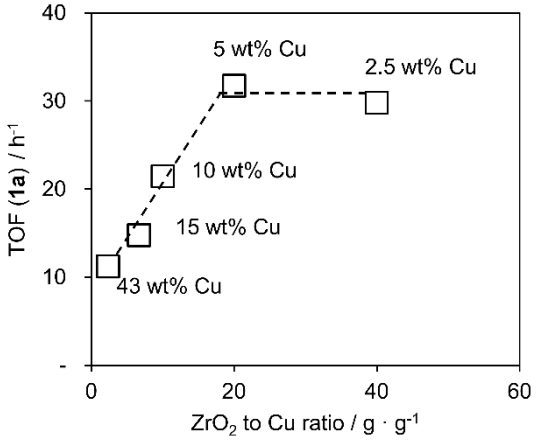

Figure 4. Effect of the ZrO_2/Cu weight ratio on the TOF of **1a** per active Cu site (by N_2O chemisorption). Substrate conversion < 40%. The initial linear part of the kinetic plot was used to calculate TOF (R^2 > 0.96). Reaction conditions: 1 mmol **1a**, 2 mmol DMAn, *o*-xylene, N_2, 120 mg Cu-ZrO_2, 190 °C.

Catalyst reusability

The simple recoverability of the spent industrial Cu-ZrO_2 catalyst lead us to investigate catalyst reusability and potential deactivation in more detail. Table 4 shows the reaction performance of the catalyst after four consecutive cycles with intermediate catalyst separation by centrifugation. After each reaction cycle with model compound **1a** and DMAn, the catalyst was separated by centrifugation and washed twice with ethanol and once with *o*-xylene before use in a new catalytic cycle. Conversion was found to drop by 10-15% after each cycle, while selectivity remained stable during the first two cycles followed by a 9% decrease in cycle 3. In order to regenerate the catalyst after cycle 3, it was treated with hydrogen at elevated temperature (300 °C) as described in the catalyst pretreatment protocol. This regenerated catalyst, regained most of its initial activity, while selectivity was slightly lower.

In order to obtain a deeper insight into the catalyst's deactivation, the latter has been analyzed by a combination of ToF-SIMS (Cu, Zr and C surface species analysis), N_2O chemisorption (Cu active metal dispersion), TGA (organic matter) and XPS (Cu surface state). Owing to its remarkable surface sensitivity, ToF-SIMS has been

shown extremely useful for the characterization of heterogeneous catalysts, though surface analysis of adsorbed organics of spent catalysts have only been studied scarcely.[86] Table 4 summarizes the normalized intensities for Cu, Zr and organic cations as detected from the pretreated, spent and regenerated Cu-ZrO_2 catalyst surfaces. To reduce the complexity of the analysis, the more than one hundred identified organic cations (Table S3) were categorized into carbohydrate ($C_xH_y^+$), nitrogen containing ($C_xH_yN_z^+$), oxygenated ($C_xH_yO_z^+$) and cations with more than 13 carbon atoms (C_{13+}^+). This latter category was created as indicator for higher molecular weight species.

The number of Cu^+ species gradually decreases after repeated recycling with a noticeable incline after hydrogen treatment (cycle 4). This trend is also confirmed by the Cu/Zr ratio. Declining conversion can be a direct consequence of the decreasing accessibility of the surface Cu species. Indeed, N_2O chemisorption measurements confirm Cu dispersion decreased from 9.0% (pretreated) to 6.9% (after cycle 3). Catalyst regeneration with H_2 restored the Cu metal dispersion (12.4%) with even slightly increased dispersion relative to the initial pretreated catalyst. An overestimation of the surface-active Cu metal sites of the spent and regenerated catalysts is possible and can be attributed to metal re-dispersion upon consecutive oxidation/reduction treatment during N_2O chemisorption. This oxidation-reduction process is reported to effectively re-disperse Cu clusters (See note 2 in ESI).[87] For the Zr cations, no distinct trend was found by ToF-SIMS analysis. Looking at the organic species, the intensity of nitrogen containing organic species ($C_xH_yN_z^+$) increased by more than an order of magnitude upon catalyst recycling. The most abundant nitrogen containing species are $C_3H_8N^+$, $C_2H_6N^+$ and CH_4N^+ (Table S3), likely originating from the tertiary (**2a**), secondary (**3a**) and primary (**6a**) amine products. Related to this, a similar increasing trend is found for the 4,5-dimethoxybenzylic cation (Table 4), further suggesting that these detected amine species are originating from **2a**. Importantly, for the nitrogen containing species ($C_xH_yN_z^+$) and the 4,5-dimethoxybenzylic cation, the increasing trend is reversed upon catalyst regeneration, indicating that these species are effectively removed by this treatment. After repeated catalyst recycling (cycle 2 and cycle 3), a small decline is noticed for the oxygenated ($C_xH_yO_z^+$) and hydrocarbon ($C_xH_y^+$) species, relative to pretreated and regenerated Cu-ZrO_2. Thus, these species do not seem to accumulate on the catalyst surface. Catalyst deactivation caused by increased fouling by larger side products (represented by C_{13+}^+) is disproved by ToF-SIMS, as the C_{13+}^+ intensity remains relatively low and nearly constant upon catalyst recycling. Noteworthy, no copper nitrides (Cu_3N) species were detected by ToF-SIMS on the spent catalysts. Metal nitride formation has though been reported as important deactivation mechanism for Cu-based catalyst in presence of alkylamines, although at higher temperature (240 °C) and in a gas phase reactions.[60] Overall, ToF-SIMS and N_2O chemisorption demonstrate that incomplete desorption of the aminated reaction product and a reduced number of surface-active Cu metal sites lower the catalyst activity over time. Catalyst regeneration by H_2 treatment at elevated temperature provides an effective and easy solution to largely restore the catalytic activity.

The presence of adsorbed species was further investigated by TGA analysis (under N_2) of the spent (after cycle 3) and the regenerated (also after cycle 3) Cu-ZrO_2 catalyst. As shown in Figure S9, a significant larger relative mass loss was found for the spent (6.9%) Cu-ZrO_2 catalyst compared to the regenerated (4.2%). Moreover, the maximum desorption rate occurs at distinct temperatures for the spent (322 °C) and regenerated (285 °C) catalysts, indicating the presence of different adsorbed species. The spent Cu-ZrO_2 shows an additional weight loss band centered at 203 °C in the DTG profile. Clearly, these results further indicate that the regeneration step effectively reduces the number of adsorbed species.

The chemical state of the pretreated and recycled catalysts was measured by X-ray Photoelectron Spectroscopy (XPS) as shown in Table 4 (bottom) and Figure S10. Cu oxidation state can be obtained from the Cu $2p_{3/2}$ peak, centered at 934 eV. However, this peak contains multiple Cu^0, Cu^+ and Cu^{2+} components that are difficult to resolve.[88] Note that in the pretreated catalyst, the presence of Cu^0 was confirmed by XRD (Figure S4). Noteworthy, the higher energy satellite peak at 944 eV, associated with Cu^{2+} species, is present for the pretreated catalyst and after cycle 2, while lacking after cycle 3 (spent catalyst) and in the regenerated Cu-ZrO_2 after cycle 3 (Figure S10). It is possible that the applied reaction conditions (i.e., 190 °C, 1 bar H_2) are thus sufficient to reduce the Cu^{2+}. However, the total Cu surface content and the Cu/Zr ratio gradually decrease with increasing number of catalytic cycles, in good agreement with the results found by ToF-SIMS. This can be caused by the sintering of surface Cu as shown by N_2O chemisorption. Leaching of surface Cu into the reaction mixture was ruled out by the hot filtration test and the ICP measurements (*vide supra*). An alternative hypothesis would be that the adsorbed species after reaction selectively cover the Cu sites, rather than the Zr sites. Related to this, the number of Cu^0 and Cu^+ species slightly lowered upon recycling, with a small increase after regeneration. With Cu^0 being essential for the HB reaction, these results imply that the reduced number of active Cu surface sites is responsible for the reduced catalyst activity.

Table 4. Recycling of Cu-ZrO_2 catalyst during HB of **1a**. **Top)** Alcohol **1a** conversion and **2a** selectivity upon recycling[a] **Middle)** Normalized intensities obtained by ToF SIMS on the Cu-ZrO_2 catalyst surface after cycles of **1a** HB with DMAn. The fragments are summed up in categories. Detected intensities are normalized by dividing

by total cation count minus the Na^+ intensity. Each sample was analyzed on three different spots. The average with standard error is reported. **Bottom)** Surface atomic concentrations in atom% (with exclusion of H) as measured by XPS of the catalyst surface.

	Cycle 1	**Cycle 2**	**Cycle 3**	**Cycle 4[b]**
Conv. / %	95	87	77	89
Select. / %	97	97	88	90
ToF SIMS normalized intensities (± SD)				
Catalyst after:	**Pre-treatment**	**Cycle 2**	**Cycle 3**	**Cycle 3 + regeneration**
Cu^+ (10^{-2})	21.3 ± 0.4	15.6 ± 0.3	11.1 ± 0.1	12.5 ± 0.7
Zr^+ (10^{-2})	6.1 ± 0.2	6.1 ± 0.3	9.4 ± 0.5	6.7 ± 0.8
$C_xH_yN_z^+$ (10^{-2})	0.20 ± 0.02	3.2 ± 0.2	4.2 ± 0.4	0.88 ± 0.06
$C_xH_yO_z^+$ (10^{-2})	4.8 ± 0.2	3.5 ± 0.2	3.1 ± 0.2	4.9 ± 0.5
$C_xH_y^+$ (10^{-2})	8.51 ± 0.07	8.0 ± 0.2	7.3 ± 0.2	9.7 ± 0.8
C_{13+}^+ (10^{-3})	0.43 ± 0.02	0.49 ± 0.02	0.47 ± 0.01	0.64 ± 0.03
$C_9H_{11}O_2^+$ (10^{-3})	0.12 ± 0.01	1.02 ± 0.06	1.5 ±0.1	0.25 ± 0.03
Cu/Zr	3.5 ± 0.1	2.5 ± 0.1	1.18 ± 0.07	1.8 ± 0.3
XPS surface atomic concentration (atom%)				
Cu (II)	7.3	8.7	0.5	0
Cu (0) + (I)	16.3	15.8	11.0	13.5
Total Cu	23.6	24.5	11.5	13.5
Zr	7.7	9.0	14.2	13.1
Cu/Zr	2.8	2.5	0.8	1.0

[a] Reaction conditions: 1 mmol **1a**, 2 mmol DMAn, *o*-xylene, 120 mg Cu-ZrO_2 (43 wt%), 1 bar H_2, 190 °C, 5h. [b] Prior to reaction, catalyst was regenerated with H_2 as described under catalyst pretreatment (Experimental section).

Conclusion

The success of future biorefineries is inextricably linked to optimal valorization of the obtained bio-based platform chemicals towards valuable compounds. In this context, we have successfully developed a catalytic strategy for the conversion of lignin model alcohol 3-(3,4-dimethoxyphenyl)-1-propanol (**1a**) into tertiary amines through hydrogen borrowing with secondary amines. Evaluation of a large set of industrial transition metal catalysts brought forward Cu-ZrO_2 as the most suitable catalyst for the model coupling of **1a** with DMAn. Subsidiary parameter optimization resulted in an excellent tertiary amine **2a** selectivity (97%) at nearly full alcohol conversion (95%). Low pressure hydrogen was key to high tertiary amine yield in order to reduce secondary amine **3a** and amide **4a** side products and keep the catalyst in its active state. The reaction protocol could be successfully applied to other secondary amine reactants with the highest yields for DMAn (92%) and cyclic aliphatic amines (78-86%). The combination of (i) processes parameter variation (catalyst loading, amine equivalents, temperature, and H_2 pressure) (ii) kinetic profile analysis, (iii) intermediate and side product identification and (iv) amine reactant screening allowed for the construction of an extensive reaction network to both desired and undesired products. Importantly, the actual lignin-derived monomers, 3-(4-hydroxyphenyl)-1-propanol **1p** and dihydroconiferyl alcohol **1g,** were converted to their *N,N*-dimethylamino derivative in very good yields of 85% and 78%, resp., the highest reported values thus far. As indicated by TPR, the highest TOF values were achieved with highly dispersed Cu particles in strong contact with the ZrO_2 support. In a final part, catalyst reuse was examined by recycling

experiments and analysis of the spent Cu-ZrO_2 by ToF-SIMS, N_2O chemisorption, TGA and XPS. Incomplete desorption of the product amines and a reduced number of active surface Cu sites resulted in reduced catalyst activity upon catalyst reuse. H_2 treatment at elevated temperature of the spent catalyst, largely reversed this negative effect.

Overall, this methodology can serve as an efficient upgrading strategy of lignin-derived monomers to high value tertiary *N*,*N*-disubstituted-arylalkanamines. With the promising results obtained here for the aliphatic amination of lignin monomers, ongoing work focusses on amination of actual fractionated lignin oil streams and study of the anti-oxidant capacity of these tertiary amines.

Experimental Section

Materials

For a list of all used chemicals and materials and more details on product characterization, the reader is kindly referred to the ESI.

Catalyst preparation

In addition to the commercial Cu-ZrO_2 (43 wt% Cu) catalyst, four Cu-ZrO_2 catalyst were prepared by incipient wetness impregnation with various Cu metal loading (2.5, 5.0, 10.0, 15.0 wt%). For this, 3 g monoclinic ZrO_2 (S_{bet} = 95 m²/g, V_{pore} = 0.385 ml/g) was impregnated with a aqueous $Cu(NO_3)_2{\cdot}(H_2O)_3$ solution (V = 1.16 ml) with the correct amount of Cu. Next, the catalyst was placed in a sonication bath for 45 minutes, followed by a drying step at 90°C for 12h. Afterwards, the catalyst was calcined in air at 350 °C (1h, 5 °C · min^{-1}) followed by a reduction under H_2 flow (60 ml · min^{-1}) at 350 °C (3h, 5 °C · min^{-1}).

Catalyst pretreatment

During pretreatment, the catalyst was loaded in a quartz U-tube and a H_2 flow of 60 mL min^{-1} was established. Temperature was increased (3 °C min^{-1}) to 120 °C and held for 30 min. Next, the temperature was increased (5 °C min^{-1}) to 300 °C for Cu, Pd and Ru catalyst and 500 °C for Co and Ni catalyst and held for 120 min. Finally, the catalyst bed was cooled to room temperature (RT) before loading into the reaction vessel under N_2 atmosphere.

Catalyst characterization

N_2O adsorption was performed to determine the metal dispersion of Cu catalyst. Measurements were done using a home-made flow instrument, equipped with a Pfeiffer Omnistar quadrupole mass spectrometer and the protocol was adapted from elsewhere[89]. Typically, 50 mg of metal oxide pre-catalyst was pretreated with He for 1 h at 300 °C (ramping rate of 5 °C min^{-1}). Afterwards, the sample was flushed with helium and cooled to 50 °C. Then, the sample was heated to 400 °C at a ramping rate of 7 °C min^{-1} in a reducing mixture (5% H_2 in N_2, 20 ml min^{-1}) flow to obtain the H_2-TPR profile (= TPR_1). Afterwards, the sample was cooled to 60 °C under a He flow. Next, a pure N_2O flow was installed (7 mL min^{-1}) for 30 min to oxidize the surface Cu metal species. Afterwards, the sample was cooled to 50 °C and flushed with He (15 ml min^{-1}) for 30 min, after which a second H_2-TPR profile (= TPR_2) was obtained in an identical way as before. Dispersion (D) was calculated based on hydrogen consumption (A) as in Equation 1.

$$D_{Cu} = \frac{2\,A_{TPR2}}{A_{TPR1}} \times 100\% \quad \text{(Eq. 1)}$$

The catalyst surface was analyzed by time of flight secondary ion mass spectrometry (ToF-SIMS) with a ToF-SIMS instrument from IONTOF GmbH as reported elsewhere.[90] Catalyst powders were pressed onto the adhesive part of Post-it papers. A pulsed Bi_5^+ metal ion source was used to produce a primary beam at an acceleration voltage of 30 kV. An ac target current of 0.1 pA with a bunched pulse width lower than 1 ns was used. A raster of 128 × 128 data points over an area of 250 × 250 µm² was used. The total primary ion beam dose for each analyzed area was kept below 7×10^{10} ions cm^{-2}, ensuring static conditions. A lateral resolution of ~3 µm and mass resolution m/Δm > 4000 at m/z 29 were maintained for spectral acquisition. Charge compensation was done by an interlaced electron flood gun (Ek = 20 eV). Data analyses were carried out with the SurfaceLab software (version 6.5.0). Cu content in the reaction mixture was measured by inductively coupled plasma-atomic emission spectrometer (ICP-AES, PerkinElmer Optima 3300 DV, Cu emission at 327.4 nm). The reaction mixture obtained after General procedure 1 was filtered and concentrated *in vacuo*. The concentrated sample was dissolved using 8 mL aqua regia for 2h at 70 °C and diluted using 0.42 M HNO_3 in water before ICP measurement. Elemental analysis of catalyst was performed by sequential WDXRF analysis on a Bruker S8 TIGER 5 kW instrument with rhodium anode. Powders are pulverized to a fineness of 40 µm or below and analyzed in a liquid cup (7g). The multipurpose and standardless quant-express protocol was used. The structure of the Cu-ZrO_2 catalyst and CuO-

ZrO_2 pre-catalyst was determined by X-ray powder diffraction (PXRD) on a high-throughput STOE STADI P Combi diffractometer in transmission mode with focusing Ge(111) monochromatic X-ray inlet beams ($\lambda = 1.5406$ Å, Cu Kα source). XPS measurements were carried out on a SSX 100/206 photoelectron spectrometer (Surface Science Instruments) equipped with a monochromatized Al-Kα radiation source (1486 eV). The sample powders, pressed in small stainless troughs of 4 mm diameter, were placed on an insulating homemade ceramic carousel. The pressure in the analysis chamber was around 10−6 Pa. The analyzed area was ~1.4 mm², and the pass energy was set at 150 eV. Data treatment was performed with the CasaXPS program (Casa Software Ltd., UK); spectra were decomposed with the least-squares fitting routine provided by the software with a Gaussian/Lorentzian (85/15) product function after the baseline was subtracted. TGA was performed using a Mettler Toledo TGA/DSC 3+ under a N_2 (90 mL min^{-1}) flow. Typically, about 10-15 mg of the dried sample (80 °C) was weighted in an alumina sample holder and heated to 800 °C at 10 °C min^{-1}.

Representative reaction procedure (General procedure 1)

Typically, a 50 mL stainless steel Parr reactor was charged with 1 mmol 3-(3,4-dimethoxyphenyl)-1-propanol (**1a**), 0.1 g dodecane internal standard and 20 mL *o*-xylene solvent. Next, 120 mg catalyst was added under nitrogen atmosphere. For the commercial Cu-ZrO_2 (43 wt%), this corresponds to 7 mol% of active Cu (as measured by N_2O chemisorption) *versus* the substrate. After sealing, the reaction vessel was flushed three times with nitrogen. Then, 2 mmol DMAn was fed to the reactor using a mass flow controller and the reactor was pressurized with nitrogen and a total pressure of 10 bar (relative to vacuum). A stirring rate of 1400 rpm was applied and the reactor vessel was heated at 6.3 °C min^{-1} to 190 °C and the reaction time started once the desired temperature was reached. After reaction, the reaction vessel was cooled to 25 °C by an ice-water bath. Next, the reaction mixture and catalyst were collected and the empty reaction vessel was rinsed twice with ethanol, which was collected as well. The catalyst was separated by centrifuging and the resulting mixture was analyzed by GC-FID and GC-MS.

Acknowledgements

DR, BUWM and BS acknowledge funding through EoS project BIOFACT and iBOF project Next-BIOREF. BUWM and DPD are Collen-Francqui research professors of the Francqui foundation. The authors kindly thank Michiel Aerts for the TGA measurements and Pierre Eloy for the XPS measurements.

Conflict of Interest

The authors declare no conflict of interest.

Data Availability Statement

The data that support the findings of this study are available from the corresponding author upon reasonable request.

Keywords: Amination • Hydrogen transfer • Lignin • Heterogeneous catalysis • tertiary amines

References

[1] K. Holmberg, in *Ullmann's Encycl. Ind. Chem.*, Wiley-VCH Verlag GmbH & Co. KGaA, Weinheim, 2019, **2019**, pp. 1–56.

[2] P. Roose, K. Eller, E. Henkes, R. Rossbacher, H. Höke, in *Ullmann's Encycl. Ind. Chem.*, Wiley-VCH Verlag GmbH & Co. KGaA, Weinheim, 2015, Germany, **2015**, pp. 1–55.

[3] 2019 World Health Organization, World Health Organization Model List of Essential Medicines, 21st List, Geneva, **n.d.**

[4] S. A. Greene, *Sittig's Handbook of Pesticides and Agricultural Chemicals*, Elsevier, 2007, **2007**.

[5] N. A. McGrath, M. Brichacek, J. T. Njardarson, *J. Chem. Educ.* **2010**, *87*, 1348–1349.

[6] J. Rodrigalvarez, M. Nappi, H. Azuma, N. J. Flodén, M. E. Burns, M. J. Gaunt, *Nat. Chem.* **2020**, *12*, 76–81.

[7] A. W. Von Hofmann, *Philos. Trans. R. Soc. London* **1850**, 14093–131.

[8] D. B. Bagal, B. M. Bhanage, *Adv. Synth. Catal.* **2015**, *357*, 883–900.

[9] L. Huang, M. Arndt, K. Gooßen, H. Heydt, L. J. Gooßen, *Chem. Rev.* **2015**, *115*, 2596–2697.

[10] J. R. Cabrero-Antonino, R. Adam, V. Papa, M. Beller, *Nat. Commun.* **2020**, *11*, 3893.

[11] H. Goksu, H. Sert, B. Kilbas, F. Sen, *Curr. Org. Chem.* **2017**, *21*, 794–820.

[12] R. Kumar, N. J. Flodén, W. G. Whitehurst, M. J. Gaunt, *Nature* **2020**, *581*, 415–420.

[13] T. Irrgang, R. Kempe, *Chem. Rev.* **2020**, *120*, 9583–9674.

[14] W. Faveere, T. Mihaylov, M. Pelckmans, K. Moonen, F. Gillis-D'Hamers, R. Bosschaerts, K. Pierloot, B. F. Sels, *ACS Catal.* **2020**, *10*, 391–404.

[15] A. K. Bains, A. Kundu, S. Yadav, D. Adhikari, *ACS Catal.* **2019**, *9*, 9051–9059.

[16] S. Bähn, S. Imm, L. Neubert, M. Zhang, H. Neumann, M. Beller, *ChemCatChem* **2011**, *3*, 1853–1864.

[17] K. Shimizu, *Catal. Sci. Technol.* **2015**, *5*, 1412–1427.

[18] M. Pelckmans, T. Renders, S. Van de Vyver, B. F. Sels, *Green Chem.* **2017**, *19*, 5303–5331.

[19] V. Froidevaux, C. Negrell, S. Caillol, J.-P. Pascault, B. Boutevin, *Chem. Rev.* **2016**, *116*, 14181–14224.

[20] K. I. Shimizu, K. Kon, W. Onodera, H. Yamazaki, J. N. Kondo, *ACS Catal.* **2013**, *3*, 112–117.

[21] P. T. Anastas, J. B. Zimmerman, *Environ. Sci. Technol.* **2003**, *37*, 94A-101A.

[22] F. Bahé, L. Grand, E. Cartier, M. Jacolot, S. Moebs-Sanchez, D. Portinha, E. Fleury, F. Popowycz, *European J. Org. Chem.* **2020**, 599–608.

[23] J. Jeong, K. I. Fujita, *J. Org. Chem.* **2021**, *86*, 4053–4060.

[24] M. H. S. A. Hamid, C. L. Allen, G. W. Lamb, A. C. Maxwell, H. C. Maytum, A. J. A. Watson, J. M. J. Williams, *J. Am. Chem. Soc.* **2009**, *131*, 1766–1774.

[25] R. Labes, C. Mateos, C. Battilocchio, Y. Chen, P. Dingwall, G. R. Cumming, J. A. Rincón, M. J. Nieves-Remacha, S. V Ley, *Green Chem.* **2019**, *21*, 59–63.

[26] S. Elangovan, A. Afanasenko, J. Haupenthal, Z. Sun, Y. Liu, A. K. H. Hirsch, K. Barta, *ACS Cent. Sci.* **2019**, *5*, 1707–1716.

[27] K. O. Marichev, J. M. Takacs, *ACS Catal.* **2016**, *6*, 2205–2210.

[28] F. Kallmeier, R. Fertig, T. Irrgang, R. Kempe, *Angew. Chemie* **2020**, *132*, 11887–11891.

[29] T. Yan, B. L. Feringa, K. Barta, *Nat. Commun.* **2014**, *5*, 5602.

[30] S. Elangovan, J. Neumann, J.-B. Sortais, K. Junge, C. Darcel, M. Beller, *Nat. Commun.* **2016**, *7*, 12641.

[31] A. Baiker, W. Richarz, *Synth. Commun.* **1978**, *8*, 27–32.

[32] Y. Wu, Y. Huang, X. Dai, F. Shi, *ChemSusChem* **2019**, *12*, 3185–3191.

[33] T. Wang, J. Ibañez, K. Wang, L. Fang, M. Sabbe, C. Michel, S. Paul, M. Pera-titus, P. Sautet, *Nat. Catal.* **2019**, 1–7.

[34] T. Tong, W. Guo, X. Liu, Y. Guo, C.-W. Pao, J.-L. Chen, Y. Hu, Y. Wang, *J. Catal.* **2019**, *378*, 392–401.

[35] K. Shimizu, S. Kanno, K. Kon, S. M. A. Hakim Siddiki, H. Tanaka, Y. Sakata, *Catal. Today* **2014**, *232*, 134–138.

[36] A. Tomer, F. Wyrwalski, C. Przybylski, J.-F. Paul, E. Monflier, M. Pera-Titus, A. Ponchel, *J. Catal.* **2017**, *356*, 111–124.

[37] M. Ousmane, G. Perrussel, Z. Yan, J. M. Clacens, F. De Campo, M. Pera-Titus, *J. Catal.* **2014**, *309*, 439–452.

[38] G. Liang, Y. Zhou, J. Zhao, A. Y. Khodakov, V. V. Ordomsky, *ACS Catal.* **2018**, *8*, 11226–11234.

[39] F. Niu, S. Xie, Z. Yan, B. T. Kusema, V. V. Ordomsky, A. Y. Khodakov, *Catal. Sci. Technol.* **2020**, *10*, 4396–4404.

[40] T. Irrgang, R. Kempe, *Chem. Rev.* **2019**, *119*, 2524–2549.

[41] B. G. Reed-Berendt, D. E. Latham, M. B. Dambatta, L. C. Morrill, *ACS Cent. Sci.* **2021**, *7*, 570–585.

[42] T. I. Korányi, B. Fridrich, A. Pineda, K. Barta, *Molecules* **2020**, *25*, 2815.

[43] E. Cooreman, T. Vangeel, K. Van Aelst, J. Van Aelst, J. Lauwaert, J. W. Thybaut, S. Van Den Bosch, B. F. Sels, *Ind. Eng. Chem. Res.* **2020**, *59*, 17035–17045.

[44] Z. Sun, J. Cheng, D. Wang, T.-Q. Yuan, G. Song, K. Barta, *ChemSusChem* **2020**, *13*, 5199–5212.

[45] M. M. Abu-Omar, K. Barta, G. T. Beckham, J. S. Luterbacher, J. Ralph, R. Rinaldi, Y. Román-Leshkov, J. S. M. Samec, B. F. Sels, F. Wang, *Energy Environ. Sci.* **2021**, *14*, 262–292.

[46] T. Renders, G. Van den Bossche, T. Vangeel, K. Van Aelst, B. Sels, *Curr. Opin. Biotechnol.* **2019**, *56*, 193–201.

[47] Y. M. Questell-Santiago, M. V Galkin, K. Barta, J. S. Luterbacher, *Nat. Rev. Chem.* **2020**, *4*, 311–330.

[48] S. Van den Bosch, W. Schutyser, S.-F. Koelewijn, T. Renders, C. M. Courtin, B. F. Sels, *Chem. Commun.* **2015**, *51*, 13158–13161.

[49] K. Natte, A. Narani, V. Goyal, N. Sarki, R. V. Jagadeesh, *Adv. Synth. Catal.* **2020**, *362*, 5143–5169.

[50] Z. Sun, B. Fridrich, A. de Santi, S. Elangovan, K. Barta, *Chem. Rev.* **2018**, *118*, 614–678.

[51] Z. Sun, G. Bottari, A. Afanasenko, M. C. A. Stuart, P. J. Deuss, B. Fridrich, K. Barta, *Nat. Catal.* **2018**, *1*, 82–92.

[52] I. Kumaniaev, J. S. M. Samec, *Ind. Eng. Chem. Res.* **2019**, *58*, 6899–6906.

[53] R. E. Kirk, D. F. Othmer, J. I. Kroschwitz, M. Howe-Grant, **1992**, p. 582.

[54] R. G. Rowland, J. Dong, C. A. Migdal, in *Lubr. Addit.*, CRC Press, Third Edition. | Boca Raton : CRC Press, Taylor & Francis Group, 2017., **2017**, pp. 3–36.

[55] O. I. Dyubchenko, V. V. Nikulina, E. I. Terakh, A. E. Prosenko, I. A. Grigor'ev, *Russ. J. Appl. Chem.* **2005**, *78*, 781–786.

[56] O. I. Dyubchenko, V. V. Nikulina, E. I. Terakh, A. E. Prosenko, I. A. Grigor'ev, *Russ. Chem. Bull.* **2007**, *56*, 1149–1155.

[57] K. Kaźmierczak, A. Salisu, C. Pinel, M. Besson, C. Michel, N. Perret, *Catal. Commun.* **2021**, *148*, 1–5.

[58] X. Wang, R. Rinaldi, *ChemSusChem* **2012**, *5*, 1455–1466.

[59] J. Ibáñez, B. T. Kusema, S. Paul, M. Pera-Titus, *Catal. Sci. Technol.* **2018**, *8*, 5858–5874.

[60] A. Baiker, D. Monti, Y. S. Fan, *J. Catal.* **1984**, *88*, 81–88.

[61] X. Liu, P. Hermange, J. Ruiz, D. Astruc, *ChemCatChem* **2016**, *8*, 1043–1045.

[62] D. Ruiz, A. Aho, T. Saloranta, K. Eränen, J. Wärnå, R. Leino, D. Y. Murzin, *Chem. Eng. J.* **2017**, *307*, 739–749.

[63] Y. Liu, A. Afanasenko, S. Elangovan, Z. Sun, K. Barta, *ACS Sustain. Chem. Eng.* **2019**, *7*, 11267–11274.

[64] F. Pompeo, N. N. Nichio, M. M. V. M. Souza, D. V. Cesar, O. A. Ferretti, M. Schmal, *Appl. Catal. A Gen.* **2007**, *316*, 175–183.

[65] Y. S. Demidova, E. V. Suslov, I. L. Simakova, E. S. Mozhajcev, D. V. Korchagina, K. P. Volcho, N. F. Salakhutdinov, A. Simakov, D. Y. Murzin, *J. Catal.* **2018**, *360*, 127–134.

[66] K. V. R. Chary, K. K. Seela, D. Naresh, P. Ramakanth, *Catal. Commun.* **2008**, *9*, 75–81.

[67] N. Scotti, F. Bossola, F. Zaccheria, N. Ravasio, *Catalysts* **2020**, *10*, 168.

[68] X. Li, P. Yang, X. Zhang, Y. Liu, C. Miao, J. Feng, D. Li, *ACS Appl. Mater. Interfaces* **2021**, *13*, 22292–22303.

[69] K. Shimizu, K. Ohshima, A. Satsuma, *Chem. - A Eur. J.* **2009**, *15*, 9977–9980.

[70] P. Daw, A. Kumar, N. A. Espinosa-Jalapa, Y. Ben-David, D. Milstein, *J. Am. Chem. Soc.* **2019**, *141*, 12202–12206.

[71] A. Baiker, in *Stud. Surf. Sci. Catal.*, **1988**, pp. 283–290.

[72] A. Baiker, W. Caprez, W. L. Holstein, *Ind. Eng. Chem. Prod. Res. Dev.* **1983**, *22*, 217–225.

[73] G. Guillena, D. J. Ramón, M. Yus, *Chem. Rev.* **2010**, *110*, 1611–1641.

[74] T. A. Nigst, A. Antipova, H. Mayr, *J. Org. Chem.* **2012**, *77*, 8142–8155.

[75] T. Kanzian, T. A. Nigst, A. Maier, S. Pichl, H. Mayr, *European J. Org. Chem.* **2009**, *2009*, 6379–6385.

[76] Y. Kim, J. Heo, D. Kim, S. Chang, S. Seo, *Nat. Commun.* **2020**, *11*, 4761.

[77] P. Y. Bruice, *Organic Chemistry*, Pearson Education, **2014**.

[78] M. T. Sabatini, L. T. Boulton, H. F. Sneddon, T. D. Sheppard, *Nat. Catal.* **2019**, *2*, 10–17.

[79] H. Lu, T.-Y. Yu, P.-F. Xu, H. Wei, *Chem. Rev.* **2021**, *121*, 365–411.

[80] T. Cuypers, T. Morias, S. Windels, C. Marquez, C. Van Goethem, I. Vankelecom, D. E. De Vos, *Green Chem.* **2020**, *22*, 1884–1893.

[81] Y. ONO, *J. Catal.* **1981**, *72*, 121–128.

[82] K. Shimizu, N. Imaiida, K. Kon, S. M. A. Hakim Siddiki, A. Satsuma, *ACS Catal.* **2013**, *3*, 998–1005.

[83] K. V. R. Chary, G. V. Sagar, C. S. Srikanth, V. V. Rao, *J. Phys. Chem. B* **2007**, *111*, 543–550.

[84] Z. Liu, M. D. Amiridis, Y. Chen, *J. Phys. Chem. B* **2005**, *109*, 1251–1255.

[85] P. Baeza, G. Aguila, G. Vargas, J. Ojeda, P. Araya, *Appl. Catal. B Environ.* **2012**, *111–112*, 133–140.

[86] L.-T. Weng, *Appl. Catal. A Gen.* **2014**, *474*, 203–210.

[87] A. J. Marchi, J. L. G. Fierro, J. Santamaría, A. Monzón, *Appl. Catal. A Gen.* **1996**, *142*, 375–386.

[88] M. T. Marques, A. M. Ferraria, J. B. Correia, A. M. B. do Rego, R. Vilar, *Mater. Chem. Phys.* **2008**, *109*, 174–180.

[89] F. Dong, G. Ding, H. Zheng, X. Xiang, L. Chen, Y. Zhu, Y. Li, *Catal. Sci. Technol.* **2016**, *6*, 767–779.

[90] R. De Clercq, M. Dusselier, C. Poleunis, D. P. Debecker, L. Giebeler, S. Oswald, E. Makshina, B. F. Sels, *ACS Catal.* **2018**, *8*, 8130–8139.